



# A simple fabrication of superhydrophobic PVDF/SiO<sub>2</sub> coatings and their anti-icing properties

Xinyu Tan<sup>1,2,a)</sup>, Zhengtao Huang<sup>2</sup>, Lihua Jiang<sup>2</sup>, Ting Xiao<sup>2</sup>, Yunkuan Wang<sup>2</sup>, Xiongbo Yang<sup>3</sup>, Heng Zhu<sup>2</sup>, Shuangshuang Li<sup>1</sup>, Xiaobo Chen<sup>4,a)</sup>

<sup>1</sup> College of Electrical Engineering and New Energy, Hubei Provincial Collaborative Innovation Center for New Energy Microgrid, China Three Gorges University, 8 Daxue Road, Yichang 443002, Hubei, China

<sup>2</sup> College of Materials and Chemical Engineering, Key Laboratory of Inorganic Nonmetallic Crystalline and Energy Conversion Materials, China Three Gorges University, 8 Daxue Road, Yichang 443002, Hubei, China

<sup>3</sup> College of Science, China Three Gorges University, 8 Daxue Road, Yichang 443002, Hubei, China

<sup>4</sup> Department of Chemistry, University of Missouri–Kansas City, Kansas City, MO 64110, USA

<sup>a)</sup> Address all correspondence to these authors. e-mails: tanxin@ctgu.edu.cn; chenxiaobo@umkc.edu

Received: 26 August 2020; accepted: 24 November 2020; published online: 13 January 2021

Xiaobo Chen was an editor of this journal during the review and decision stage. For the JMR policy on review and publication of manuscripts authored by editors, please refer to <http://www.mrs.org/editor-manuscripts/>.

Superhydrophobic coatings have been regarded as potential promising solutions to many problems, e.g., ice accumulation in the winter seasons. To be practically useful and economically attractive, it is necessary to fabricate such coatings using facile methods, i.e., with minimal steps and low cost. In this work, a polyvinylidene fluoride (PVDF)/SiO<sub>2</sub> coating is successfully prepared with a simple dip coating method. It shows impressive superhydrophobic properties with a large water contact angle (WCA) of 159° and a small sliding angle (SA) of less than 3°. Meanwhile, its superhydrophobic properties are robust in a large temperature range of – 30 to 350 °C and in various environments. Moreover, it shows remarkable anti-icing properties by delaying the freezing time (4 times) and reducing (40%) the adhesion of the ice on the substrate. Therefore, this work has displayed a promising approach for fabricating superhydrophobic coatings towards anti-icing applications.

## Introduction

Ice accumulation in winter seasons can cause severe problems for roads, automobiles, airplanes, and electrical transmission lines [1–4]. For example, it can lead to the collapse of the electrical transmission lines and towers, resulting in the loss of electricity [5], and the corrosion of metals in long-term exposure. Therefore, it is necessary to reduce ice accumulation [6, 7]. Over the past few decades, two methods have been investigated for this purpose: namely, passive [8] and active de-icing methods. The latter mainly includes manual washing, salt melting and hot melting [9], which although are effective, but consume a lot of manpower/resources. Passive methods includes the development of icephobic coatings to reduce the adhesion between the ice crystals and the substrate by making the surface of the substrate as waterless as possible [10].

One way to doing that is to make the surface water-repellent or superhydrophobic. Inspired by the lotus leaf in 1997,

Barthlott et al. [11] showed a superhydrophobic surface, which led to the hope for anti-icing [12–15].

Superhydrophobic surfaces have been prepared with many methods such as chemical vapor deposition (CVD) [16], electrospinning, etching [17], layer-by-layer deposition [18], and sol–gel methods [19], and have displayed promising results in self-cleaning [20], anti-icing [21], anti-fog [22], anti-corrosion [23], oil–water separation [24] and so on. In spite of the much progress in anti-icing [25–27], problems remain for practical applications due to high cost of raw materials, poor weather resistance, unrobust performance, and complicated fabricating methods.

In this paper, a facile one-step dip-coating method is reported in making such a superhydrophobic coating with a PVDF/SiO<sub>2</sub> composite. PVDF is chosen for its good chemical aging resistance, fatigue resistance and processibility [28–35]. Superhydrophobic coatings have been reported with PVDF/SiO<sub>2</sub>

composite [32, 33]. For example, superhydrophobic PVDF/SiO<sub>2</sub> coatings were reported using electrospinning method by Sun et al. [32] and using a nonsolvent-induced phase inversion process by Toh et al. [33]. These coatings showed impressive performance for anti-icing applications, and inspired us to develop cost-effective methods since those methods were either complicated or very costly for large-scale applications. It is known that dip coating is a straightforward method and can be applied to a large surface with low cost. Therefore, in this study, a PVDF/SiO<sub>2</sub> coating is explored with dip-coating and its superhydrophobic properties are studied in details, eyeing towards anti-icing applications.

## Results and discussion

### Structural and chemical properties of the PVDF/SiO<sub>2</sub> composite coating

The surface morphologies of the pure PVDF coating and the superhydrophobic SiO<sub>2</sub>/PVDF coating were shown in Fig. 1. The PVDF coating (Fig. 1a) was featured with a three-dimensional (3D) porous network structure having pore sizes ranging from tens of nanometers to a few micrometers (Fig. 1b) and wall

size of tens of nanometers. In contrary, the PVDF/SiO<sub>2</sub> coating showed a complete coverage with small SiO<sub>2</sub> nanoparticles which segregated to form larger domains of various sizes (Fig. 1c), on the 3D backbone of the PVDF (Fig. 1d), thus having a nano-micro hierarchical structure with a double roughness. The distributions of C, O, F, and Si were uniform, and F appeared in PVDF/SiO<sub>2</sub> coating as shown in the elemental mapping in Fig. 1e–h. To assess the roughness uniformity of the PVDF/SiO<sub>2</sub> coating, the root mean square (RMS) roughness of the sample was obtained with AFM measurements, as shown in Fig. 2. As observed, the RMS value were 180.1, 174.5, and 170.2 nm at three different locations of the sample, showing an average RMS value of 174.9 nm. These AFM images indicated that a large surface roughness was achieved for the PVDF/SiO<sub>2</sub> coating, which was beneficial for the superhydrophobicity of the coating.

The FTIR spectra of PVDF and PVDF/SiO<sub>2</sub> solution were displayed in Fig. 3. The absorption peaks at 2710, 1755 and 1340 cm<sup>-1</sup> were related to the stretching vibrations of amides groups in DMF. The absorption peaks at 910 and 850 cm<sup>-1</sup> were the Si–O–Si anti-symmetric and symmetric stretching vibrations of SiO<sub>2</sub>. Compared with the pure PVDF solution, the new peaks

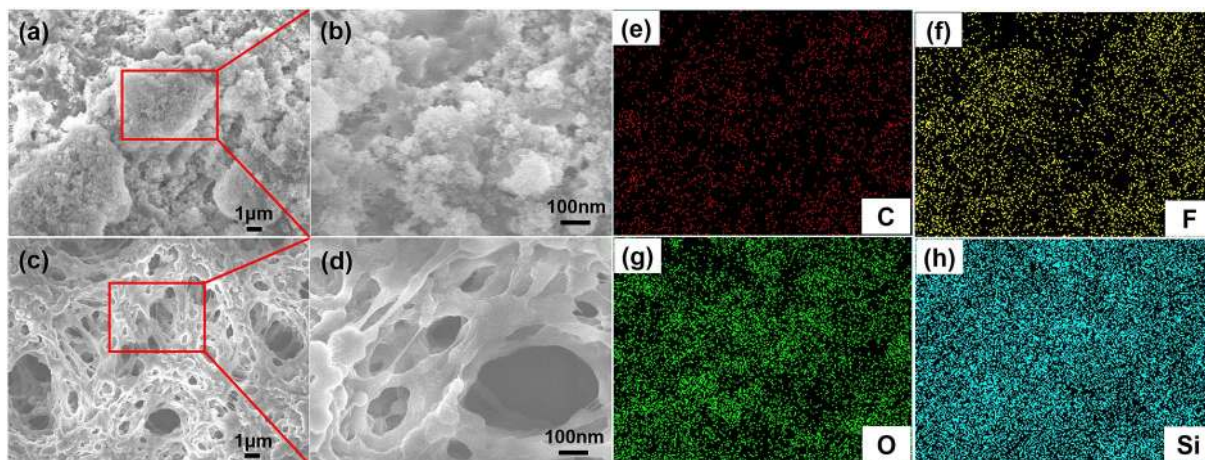


**Figure 1:** The morphologies of the surfaces under different magnifications: (a) SEM image of the PVDF coating, (b) The enlarged view of the red box in (a), (c) SEM image of the PVDF/SiO<sub>2</sub> coating, (d) The enlarged view of the red box in (c). the elemental mapping analysis of PVDF/SiO<sub>2</sub> coating; (e): C. (f): F. (g): O. (h): Si.

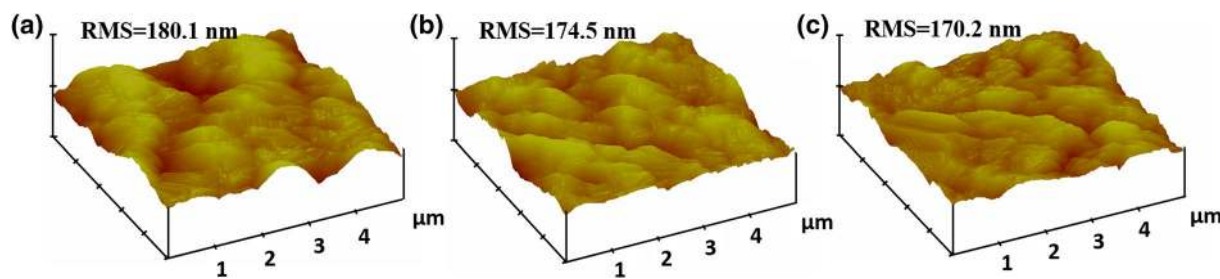


**Figure 2:** 3D (a, b, c) AFM images of PVDF/SiO<sub>2</sub> coating at three different locations.

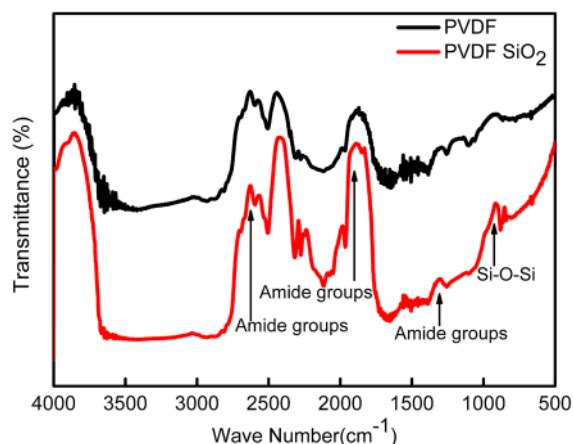


**Figure 3:** FTIR of PVDF (the top line) and PVDF- SiO<sub>2</sub> (the bottom line) solution.

of Si-O-Si groups demonstrated that the SiO<sub>2</sub> NPs and PVDF was well bond together.

**Surface wettability, weather resistance and thermal stability of the PVDF/SiO<sub>2</sub> coating**

In this part, the influence of amount of SiO<sub>2</sub> on hydrophobicity of PVDF/SiO<sub>2</sub> composite coating was studied. As shown

in Fig. 4a, along with the increase of SiO<sub>2</sub>, the WCA increased and the sliding angle decreased, regardless of the type of the substrate: glass, aluminum or plastic. On the plastic coating, the WCA increased from 95° to 110, 150 and 159° when the content of SiO<sub>2</sub> increased from 0 to 1.0, 1.97 and 6.5 wt%, respectively. Meanwhile, the sliding angle decreased from 40° to 35, 15 and 2°. Similar results were observed on the coatings on the aluminum and glass substrates. The slight difference in the WCA of the PVDF/SiO<sub>2</sub> composite coatings on these substrates might be due to the slight variation of surface roughness resulted from the variation of the roughness of the substrates. Regardless of that small variation of the WCAs, superhydrophobicity was consistently observed on those various substrates. The enhanced hydrophobicity performance with the content of the SiO<sub>2</sub> was likely due to the increased roughness of the formed nano-micro hierarchical structure when the SiO<sub>2</sub> content increased. The increase in the WCA and the decrease in the SA of the substrates were insignificant after the SiO<sub>2</sub> concentration greater than 6.5 wt%. While the SiO<sub>2</sub> concentration was greater than 10 wt%, cracks were observed on the surface of the coating, resulting in a slight decrease in WCA and a slight increase in SA. Therefore, when the SiO<sub>2</sub> content was 6.5 wt%, the coating had the best performance.

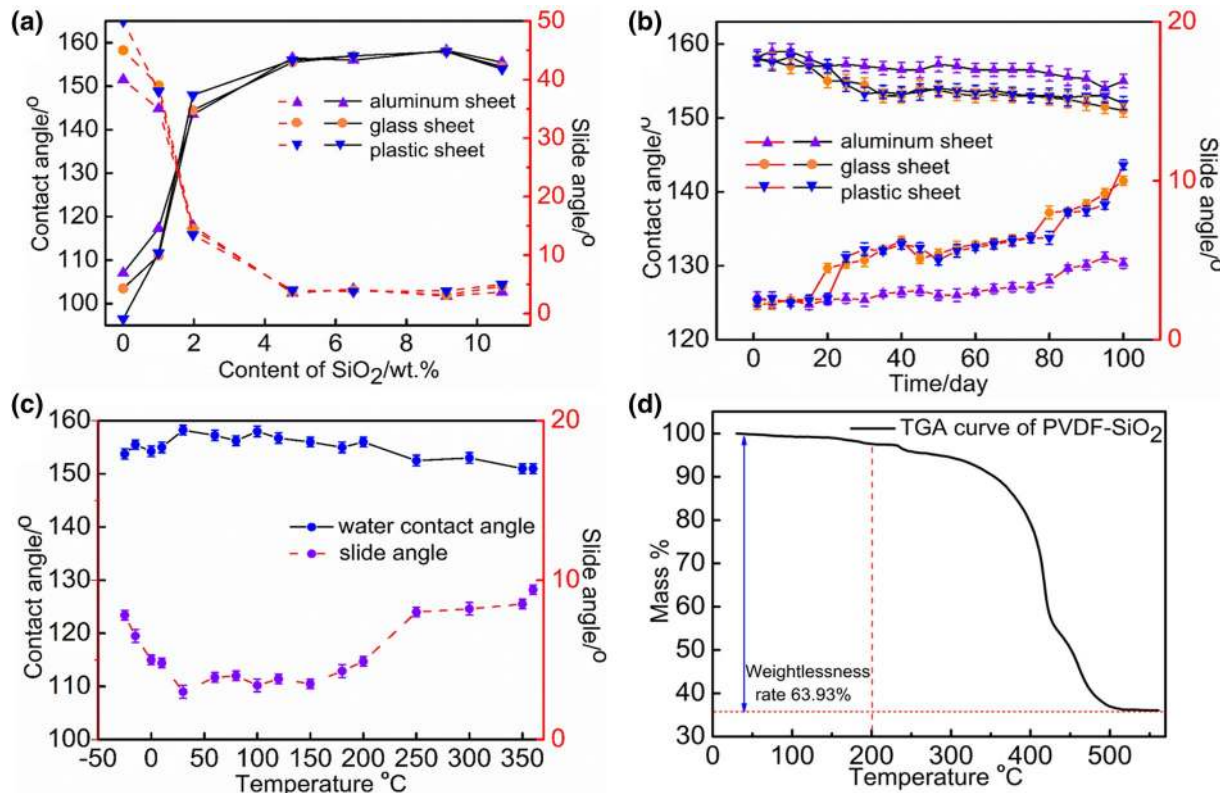


**Figure 4:** Influences of (a) the SiO<sub>2</sub> content and (b) the outdoor exposure time on the wettability of the PVDF/SiO<sub>2</sub> composite coating. Effect of treating temperature on the coating; (c): The change of WCA with the treating temperature of the sample, (d): thermogravimetric analysis curve of PVDF-SiO<sub>2</sub>.

To evaluate the adaptability of the PVDF/SiO<sub>2</sub> coatings to the outdoor environment, a long-term test was conducted from June 2019 to September 2019. The changes in WCAs and SAs over time were shown in Fig. 4b for the coatings on the glass, aluminum and plastic substrates. After 100 days outdoor exposure, the WCA remained above 153° even though small decreases were also observed (from 159° to 153° for the coating on the glass and plastic substrates, from 159° to 155° for the coating on the aluminum substrate), and the SA value increased over time (from 2° to 11° for the coating on the glass and plastic substrates, from 2° to 5° for the coating on the aluminum substrate). The coating on the aluminum substrate showed slight better performance than on the glass and plastic substrates (larger WCA and smaller SA). The changes of the WCAs and SAs over time were likely due to the UV irradiations and dust accumulations in the outdoor environment, where the summer climate in Yichang, central China, was characterized by strong sunlight, large air pollution, high temperature, high humidity and frequent rainstorms. Nevertheless, the results exhibited that a good hydrophobicity was maintained on the PVDF/SiO<sub>2</sub> coating in a real, harsh and constantly changing outdoor environment.

Due to the high stability of PVDF at low and high temperatures, the PVDF/SiO<sub>2</sub> coating was expected to have a stable hydrophobicity performance against temperature change. To test that, 16 samples were placed in a thermostat in the temperature range of -30 °C to 350 °C with a step of about 20 °C for half an hour, and WCAs and SAs were measured after the samples were cooled to room temperature. Figure 4c showed that as the treating temperature decreased from room temperature, WCA decreased and SA increased, likely due to vapor condensation on the surface under the high humidity of the air [36]; as the temperature increased from room temperature, WCA slowly decreased and SA gradually increased, partially due to gradual thermal deformation of the PVDF in the lower temperature range and thermal decomposition of PVDF in the higher temperature range. As seen from the TGA analysis in Fig. 4d, a small weight loss below 200 °C was likely due to the escape of the trapped DMF molecules and a larger weight loss above 200 °C was likely due to the thermal decomposition of PVDF. In spite of the slight decrease of the hydrophobicity at the very low and high temperature ranges, WCA larger than 150° and SA less than 10° were maintained after the coating was treated in the large temperature range of -30 to 350 °C, displaying a robust superhydrophobicity against temperature variation.

### Anti-icing performance of the PVDF/SiO<sub>2</sub> coating

To evaluate the ability of PVDF/SiO<sub>2</sub> coating to reduce ice accumulation, freezing weather was simulated at -20 °C and supercooled water (1 °C) was completely dropped on the treated and

untreated substrates at a speed of 3 mL/min (an area of 24 cm<sup>2</sup> for a single sample) until the surface of the untreated sample was completely frozen (about 10 min's spraying time). Such method has been demonstrated in our previous work [37].

Figure 5a showed the corresponding mass changes over time. The mass increased almost linearly on both surfaces. The mass of ice on the untreated aluminum increased to about 3.5 g after 6 h, while it only increased to about 1.0 g on the treated surface. Therefore, the coating reduced about 71.4% of ice formation on the surface. Figure 5b showed the surface ice formation rate. The treated surface had a rate of about 3.0 mg/min, only 30% of that of the untreated surface. To reveal the icing characteristics properties, the growth characteristics of ice were observed on a low temperature chamber. As shown in Fig. 5c, Fig. 5d showed the corresponding digital pictures. After 6 h, the untreated substrate was completely covered with ice, however, there was little ice on the treated aluminum.

To evaluate the influence of freezing/melting cycle on the hydrophobic performance, the WCA and SA of the PVDF/SiO<sub>2</sub> coated aluminum were measured after frozen at -20 °C for 2 days and then melted at room temperature for several cycles. As shown in Fig. 6a, even though WCA gradually decreased from 159° to 148° and SA gradually increased from 2° to 13.5°, as the number of freezing/melting cycle increased to 18, a good stability was still maintained. To reveal the ice adhesion properties, the escape velocity of ice was observed on a rotator. As shown in Fig. 6b, 0.5 mL water droplets were frozen on the surface, and their escape velocity were measured. Figure 6c showed the relationship between the escape velocity of ice and the number of cycles. Although, the ice escape velocity to both the coated and uncoated surface slowly increased as the number of cycle increased, it was only about 40% on coated surface of that on the uncoated surface. Therefore, the ice adhesion strength to the coated surface was reduced to only 40% of that of the untreated surface [10].

The freezing process was studied to understand the ice formation process of ice particles. Figure 6d showed that the droplets began to freeze after 25 s and were completely frozen after 65 s on the uncoated Al surface; in comparison, it only started to freeze after 116 s and were completely frozen after 273 s on the coated Al surface. Thus, the freezing time on coated surface was delayed more than 4 times than on the untreated surface.

The rate of ice formation on the surface was determined with the rates of nucleation and crystal growth. Since the nucleus was formed on the solid surface in contact with the liquid, the Gibbs free energy barrier  $\Delta G$  forming the liquid core was closely related to the inherent wettability of the surface. The free enthalpy change of the entire crystal nucleus system can be expressed as [38–40]:

$$\Delta G = V\Delta G_V + \gamma_{LX}A_{LX} - \pi r^2 \gamma_{LX} \cos \theta \quad (1)$$

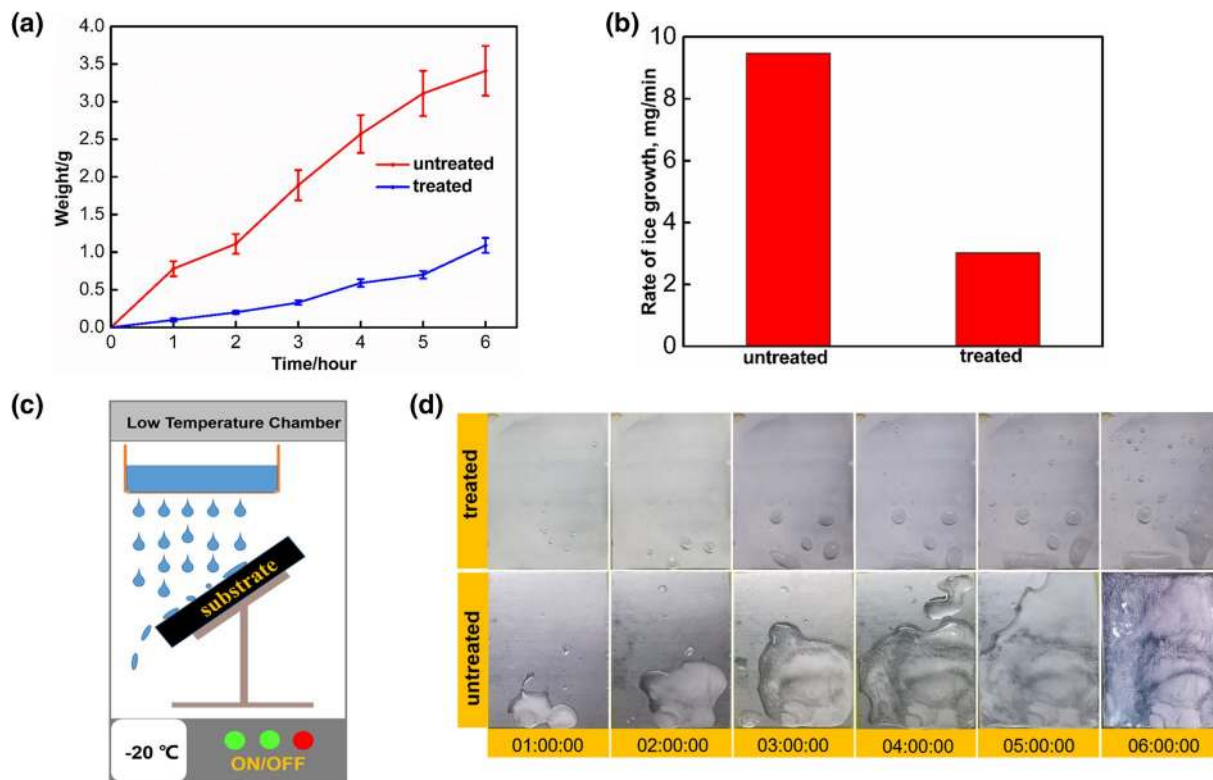


**Figure 5:** Icing properties (a): The mass changes of icing with time; (b): comparison of the growth rate of ice on untreated and treated substrates surfaces; (c): The device to measure icing characteristics of ice; (d) Comparison of the growth rate of ice on untreated and treated substrates surfaces.

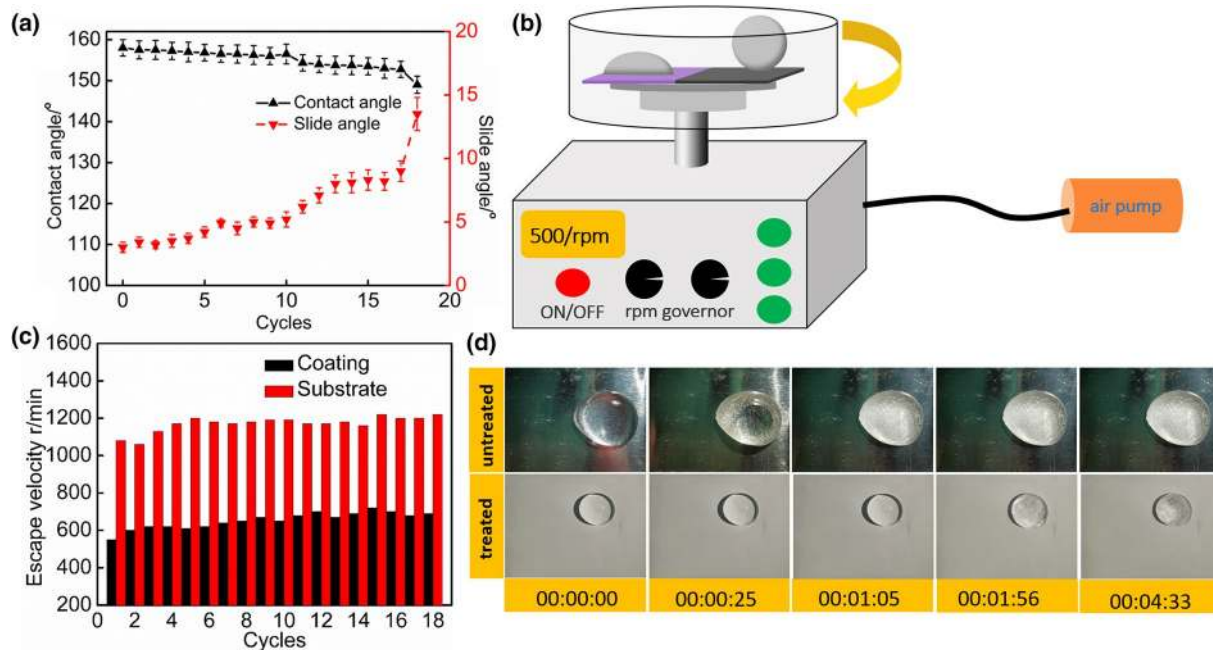


**Figure 6:** (a): The change of WCA of the PVDF/SiO<sub>2</sub> coating in 18 freeze/break cycles; (b): The device to measure ice escape velocity. (c): The ice escape velocities of the untreated (the red) and treated coating's (the black) in 18 freeze/break cycles. (d) The freezing process of 400  $\mu$ L water droplets on the untreated and treated at -20 °C.

In the Eq. (1):  $\Delta G_V$  is a free enthalpy in unit volume outside the interface energy,  $V$  is the volume of the droplet,  $\gamma_{LX}$  is the liquid-nuclear interface energy, and  $A_{LX}$  is the area of the liquid-nucleation interface,  $r$  is the radius of the droplet,  $\theta$  is the contact angle on the substrate surface in ambient water.

$$R^* = \frac{2\gamma_{LX}}{\Delta G_V} \quad (2)$$

In the Eq. (2):  $R^*$  is the critical radius of the nucleus.

Substituting Eqs. (2) into (1), Eq. (3) can be obtained as following:

$$\Delta G_h^* = \frac{16\pi\gamma_{LX}^3}{3\Delta G_V^2} \frac{(2 + \cos\theta)(1 - \cos\theta)^2}{4} \quad (3)$$

In the Eq. (3):  $\Delta G_h^*$  is the free energy required for nucleation.

When  $\theta = 0$ ,  $\Delta G_h^* = 0$ , meaning that no external energy is needed to form a critical ice core. When  $\theta = 180^\circ$ , meaning that it takes a lot of energy to form an ice core, which is equivalent to a homogeneous nucleation process. Therefore, the larger the  $\theta$ , the larger the  $\Delta G_h^*$  required for nucleation. In other words, the greater the contact angle  $\theta$ , the more difficult is to nucleate. Therefore, according to the nucleation theory [39, 40] and the heat transfer between the surface and water droplets, the superhydrophobic surface would have the function of delaying icing.

In addition, the Cassie state between the rough superhydrophobic surface and the drop indicated the presence of air pockets between the rough surface and the water drop. These air pockets could reduce the heat transfer between the water

droplets and the surface during cooling. According to Fourier's law [41], the heat transfer between solid surface and water drop was proportional to the liquid–solid area, which was minimized on a superhydrophobic surface. Therefore, the icing process was expected on a superhydrophobic surface as well.

### Acidic and alkaline resistance of the PVDF/SiO<sub>2</sub> coating

The wettability of the surface could be an important parameter for the acidic and alkaline resistance. Generally, when the surface has a WCA value above 150° and a low SA, it is difficult for droplets to stay on the surface. The acidic and alkaline resistance was usually evaluated with the WCA and SA values after immersed in the corrosive solution [42, 43]. In this work, the PVDF/SiO<sub>2</sub> coated Al was immersed in aqueous solutions with a large range of pH value from 1.0 to 12.0. Figure 7a showed that the WCA was between 151° and 158° and SA was less than 3°, when over the pH range of 1.0–12.0. WCA did not change apparently, although SA increased slightly, after 24 h soaking. After soaked for 120 h, a good superhydrophobicity remained although WCA decreased slightly to 148–155°, and SA increased to 5°–8°. This was also seen from the nearly spherical shapes of the water drops on the coated surface shown in Fig. 7b which displayed the pictures of the surfaces after 120 h of immersion in solutions with pH of 1.0, 7.0, and 12.0 (the pH was tuned with HCl, NaCl or NaOH).

The apparent nano-micro hierarchical structure of the fresh PVDF/SiO<sub>2</sub> coating (Fig. 7c) was largely maintained after 5 days'

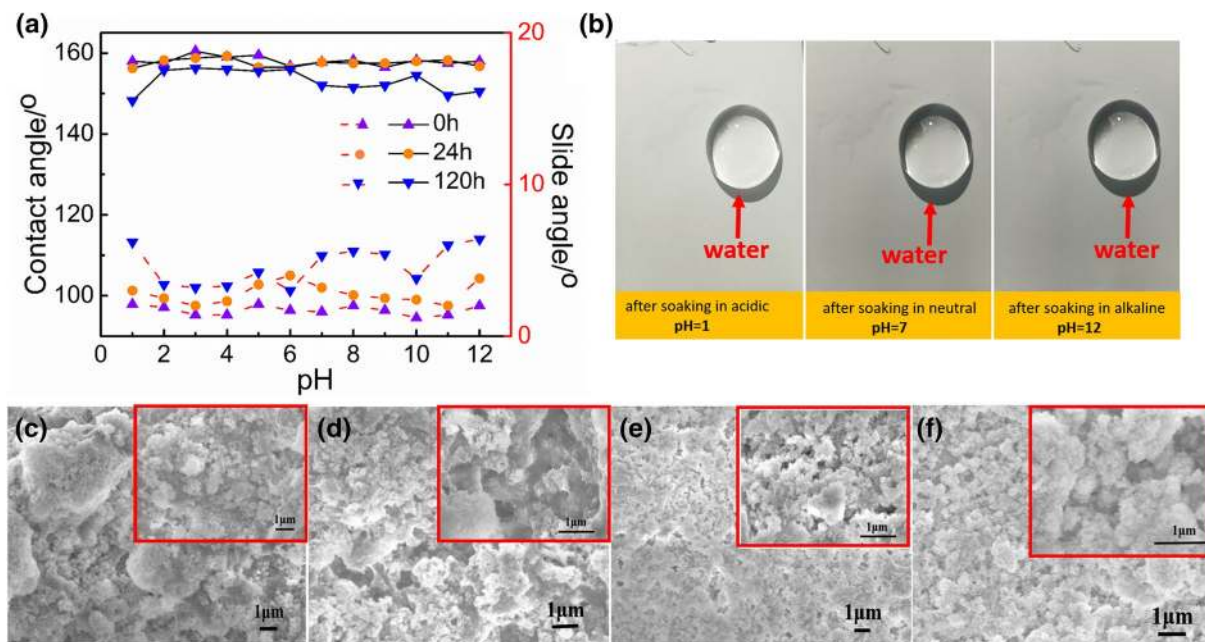


**Figure 7:** Acidic and alkaline resistance. (a): WCAs of the substrates with solutions of different pH. (b): Water droplets on the surface after 120 h of soaking in acidic, neutral, and alkaline solutions. Surface morphology of the coating: (c): before soaked in the solution, after soaked for 120 h in (d): 0.10 M HCl, (e): 3.5wt% NaCl, (f): 0.10 M NaOH.

immersion in 0.10 M HCl solution for (Fig. 7d), in 3.5 wt% NaCl solution (Fig. 7e), and in the 0.10 M NaOH solution (Fig. 7f). Therefore, the good resistance of this structure to the exposure in alkaline and acidic solutions likely enabled the robust hydrophobicity of the PVDF/SiO<sub>2</sub> coating.

## Conclusions

In summary, a superhydrophobic PVDF/SiO<sub>2</sub> composite coating is prepared with a one-step dip-coating method, showing a WCA larger than 159° and an SA smaller than 3°. Its superhydrophobic properties are maintained after exposed in outdoor environment for extended periods (e.g., 100 days), in strong corrosive environment (e.g. pH range of 1.0–12.0), over a wide temperature range (e.g., –30 to 350 °C), and after multiple icing/melting cycles. It has also displayed impressive promise in extending the freezing time (e.g., fourfold increase) and reducing the adhesion between the ice and the Al substrate (e.g., 60%). Therefore, this coating is expected to be potentially attractive for outdoor anti-icing protections, e.g. over towers, bridges and other important objects through harsh and icy winter seasons, especially with the one-step dip-coating, facile fabrication method.

## Experimental section

### Materials

Aluminum, glass and polymer plastics (polyester resin) were purchased from local store and used as substrates. PVDF

(HSV900, Mw = 6.85 × 10<sup>5</sup>) was purchased from Suzhou JILONG energy technology Ltd, China. Hexadecyltrimethoxysilane (HDTMS, ≥ 85%) was obtained from Shanghai Macklin Biochemical Technology Co., Ltd.. SiO<sub>2</sub> nanoparticles (25–35 nm) were purchased from Shanghai KEYAN Chemical Reagents Ltd, China. Absolute ethyl alcohol (EtOH, ≥ 99.5%) was purchased from Tianjin TIANLI Chemical Reagents Ltd, China. N, N-Di-methylformamide (DMF) was purchased from Sinopharm Chemical Reagent Co., Ltd. Ultrapure water with a resistivity higher than 18.2 MU cm was obtained from a three-stage Millipore Mill-Q Plus 185 purification system (Academic) and was used in all experiments.

### Preparation of PVDF/SiO<sub>2</sub> composite coating

The substrates were first cleaned with distilled water and absolute ethanol, and then dried before use. 0.30, 0.60, 1.50, 2.10, 3.0, or 3.60 g SiO<sub>2</sub> was stirred in 30 mL DMF for 6 h, then 1.50 g PVDF was added and stirred for 5 h. The substrates were immersed in this solution, then taken out, dried at 60 °C for 30 min, and sprayed with a HDTMS/EtOH solution, dried at room temperature for 20 min and then at 120 °C for 2 h. The HDTMS/EtOH solution was prepared by stirring 5 mL HDTMS in 95 mL EtOH at room temperature for 2 h. The preparation process is shown in Fig. 8.

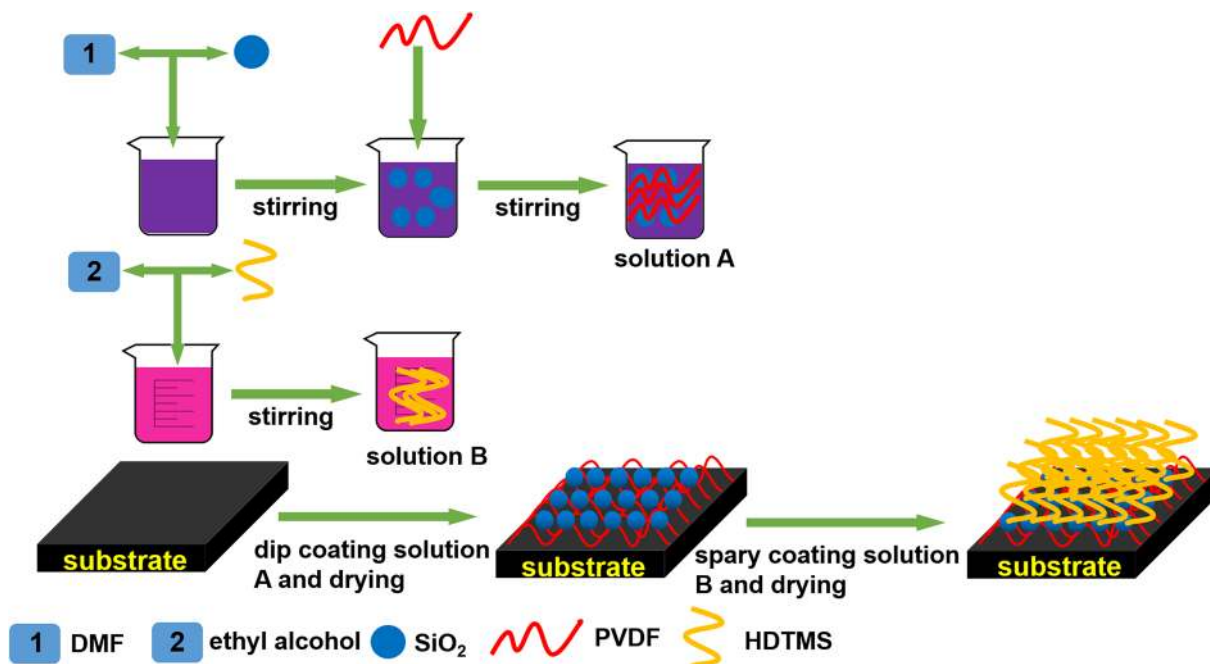


**Figure 8:** Schematic illustration of PVDF-SiO<sub>2</sub> composite coating preparation.

## Characterization

The morphologies of PVDF/SiO<sub>2</sub> coating were studied using a scanning electron microscope (FE-SEM, JSM7100F, JEOL, Japan) at 5 kV. The weight loss with temperature of coating were measured with a Synchronous thermal analyzer (TGA, STA-449-F5, Germany). The chemical property was probed with a Fourier transform-infrared spectrometer (NEXUS, Thermo Nicolet Corporation, Madison, Wisconsin) using KBr method in transmission mode in the range of 300–4000 cm<sup>-1</sup>. Static WCAs were measured at ambient temperature on a Sci3000F contact angle/interface system (Beijing Zhongchen Digital Technique Apparatus Co.,Ltd.). The surface morphology and roughness were probed with atomic force microscopy (AFM, VEECO, America).

The anti-icing properties were studied as follows. First, the substrates were cooled at – 20 °C for 60 min, and then tilted at an angle of about 20° to the horizontal plane. 100 mL supercool (0 °C) water was poured on the substrates within 1 min from a bottle located about 20 cm above. This was repeated every 30 min. The substrates' pictures were taken every hour, and the substrates were weighed to determine the amount of ice left on the substrates. Second, the substrates were added with 400 μL water droplets, then cooled at – 20 °C to monitor the icing time. Third, after the water droplets were completely frozen, the speed of the ice falling off on the substrates were measured with a rotator.

The corrosion resistance was evaluated as followed. First, WCAs of the substrates were measured with solutions of pH from 1.0 to 12.0 (adjusted with HCl or NaOH). Second, WCAs were measured with stained water after the substrates were immersed in 0.10 M HCl, 3.5 wt% NaCl or 0.10 M NaOH for 5 days. The weather resistance were examined by measuring WCAs and SAs for over 100 days after exposed in outdoor environment. The thermal stability was examined by measuring the WCA after the samples were treated at certain temperature for 30 min.

## Acknowledgments

Xinyu Tan thanks to the students and teachers who gave support for this experiment, the support of the National Natural Science Foundation of China(U1765105, 52007104) and the 111 Project(D20015) of China. Xiaobo Chen appreciates the support from the School of Biological and Chemical Sciences, Department of Chemistry, University of Missouri–Kansas City, USA.

## Open access

This article is licensed under a Creative Commons Attribution 4.0 International License, which permits use, sharing, adaptation, distribution and reproduction in any medium or format, as long as you give appropriate credit to the original author(s)

and the source, provide a link to the Creative Commons licence, and indicate if changes were made. The images or other third party material in this article are included in the article's Creative Commons licence, unless indicated otherwise in a credit line to the material. If material is not included in the article's Creative Commons licence and your intended use is not permitted by statutory regulation or exceeds the permitted use, you will need to obtain permission directly from the copyright holder. To view a copy of this licence, visit <http://creativecommons.org/licenses/by/4.0/>.

## References

1. Y. Chao, L. Yang, X. Peng, Z. Peng, C. Wang, S. Zhao, Review of the researches on icing characteristics of transmission lines and anti-icing technologies. *High Voltage Apparatus*. **50**, 131 (2014)
2. Y. Cao, W. Tan, Z. Wu, Aircraft icing: an ongoing threat to aviation safety. *Aerosp Sci Technol*. **75**, 353 (2018)
3. D. Aydin, R. Kizilel, R.O. Caniaz, S. Kizilel, Gelation-Stabilized functional composite-modified bitumen for anti-icing purposes. *Ind. Eng. Chem. Res*. **54**, 12587 (2015)
4. B. Chen, X. Hu, X. Wu, Meteorological model of wire icing caused by rime and glaze based on the process judgment. *J. Appl. Meteor Sci*. **29**, 354 (2018)
5. J. Lu, J. Guo, J. Hu, Y. Li, F. Tao, Analysis of ice disasters on ultra-high-voltage direct-current transmission lines. *Nat. Hazards*. **86**, 203 (2017)
6. C.A. Knight, Adding to the antifreeze agenda. *Nature* **406**, 249 (2000)
7. F. Sicheri, D.S.C. Yang, Ice-binding structure and mechanism of an antifreeze protein from winter flounder. *Nature* **375**, 427 (1995)
8. O. Parent, A. Ilinca, Anti-icing and de-icing techniques for wind turbines: critical review. *Cold Reg. Sci. Technol*. **65**, 88 (2011)
9. S. A. Ketcham, L.D. Minsk, R.R. Blackburn, Manual of practice for an effective anti-icing program: a guide for highway winter maintenance personnel. E.J. Fleege. 1 (1996).
10. J. Peng, B. Liu, S. Gao, K. Zhu, Y. Zhao, X. Li, X. Yuan, Enhanced anti-icing properties of branched PDMS coatings with self-regulated surface patterns. *Sci. China Tech. Sci*. **63**, 960 (2020)
11. C. Neinhuis, W. Barthlott, Purity of the sacred lotus, or escape from contamination in biological surfaces. *Planta* **202**, 1 (1997)
12. P. Hao, C. Lv, F. Niu, Y. Yu, Water droplet impact on superhydrophobic surfaces with microstructures and hierarchical roughness. *Sci. China*. **57**, 1376 (2014)
13. Y. Wang, J. Xue, Q. Wang, Q. Chen, J. Ding, Verification of Ice-phobic/anti-icing properties of a superhydrophobic surface. *ACS Appl. Mater. Interfaces* **5**, 3370 (2013)
14. G. Momen, R. Jafari, M. Farzaneh, Ice repellency behaviour of superhydrophobic surfaces: effects of atmospheric icing



- conditions and surface roughness. *Appl. Surf. Sci.* **349**, 211 (2015)
15. C. Wei, B. Jin, Q. Zhang, X. Zhan, F. Chen, Anti-icing performance of super-wetting surfaces from icing-resistance to ice-phobic aspects: Robust hydrophobic or slippery surfaces. *J. Alloys Compd.* **765**, 721 (2018)
  16. X. Xiao, Y. Cheng, B.W. Sheldon, J. Rankin, Condensed water on superhydrophobic carbon films. *J. Mater. Res.* **23**, 2174 (2008)
  17. R. Scheffler, N.-S. Bell, W. Sigmund, Electrospun Teflon AF fibers for superhydrophobic membranes. *J. Mater. Res.* **25**, 1595 (2010)
  18. S.A. Mahadik, F.D. Pedraza, B.P. Relekar, V.G. Parale, G.M. Lohar, S.S. Thorat, Synthesis and characterization of superhydrophobic-superoleophilic surface. *J. Solgel Sci. Technol.* **78**, 475 (2016)
  19. H. Wang, J. Ding, Y. Xue, X. Wang, T. Lin, Superhydrophobic fabrics from hybrid silica sol-gel coatings: structural effect of precursors on wettability and washing durability. *J. Mater. Res.* **25**, 1336 (2010)
  20. M. Wang, X. Tan, Y. Tu, P. Xiang, L. Jiang, A. Yang, R. Xu, X. Chen, Self-healing PDMS/SiO<sub>2</sub>-CaCO<sub>3</sub> composite coating for highly efficient protection of building materials. *Mater. Lett.* **265**, 127290 (2020)
  21. N. Wang, D. Xiong, Y. Deng, Y. Shi, K. Wang, Mechanically robust superhydrophobic steel surface with anti-icing, UV-durability, and corrosion resistance properties. *ACS Appl. Mater. Interfaces* **7**, 6260 (2015)
  22. J. Li, J. Zheng, J. Zhang, J. Feng, Fabrication of TiO<sub>2</sub>/PU superhydrophobic film by nanoparticle assisted cast micromolding process. *J. Nanosci. Nanotechnol.* **16**, 5875 (2016)
  23. V. Ignasi, L. Jose, B. Salvador, Superhydrophobic copper surfaces with anticorrosion properties fabricated by solventless CVD methods. *ACS Appl. Mater. Interfaces* **9**, 1057 (2016)
  24. X. Miao, L. Han, L. Wang, M. Wang, X. Sun, X. Zhu, B. Ge, Preparation of PDVB/TiO<sub>2</sub> composites and the study on the oil-water separation and degradation performances. *Sci. China Tech. Sci.* **62**, 1217 (2019)
  25. L. Wang, Q. Gong, S. Zhan, L. Jiang, Y. Zheng, Robust anti-icing performance of a flexible superhydrophobic surface. *Adv. Mater.* **28**, 7729 (2016)
  26. P. Guo, Y. Zheng, M. Wen, C. Song, Y. Lin, L. Jiang, Icephobic/anti-icing properties of micro/nanostructured surfaces. *Adv. Mater.* **24**, 2642 (2012)
  27. Y. Wang, J. Xue, Q. Wang, Q. Chen, J. Ding, Verification of ice-phobic/anti-icing properties of a superhydrophobic surface. *ACS Appl Mater Interfaces.* **5**, 3370 (2013)
  28. W. Zhang, Z. Shi, F. Zhang, X. Liu, J. Jin, L. Jiang, Superhydrophobic and superoleophilic PVDF membranes for effective separation of water-in-oil emulsions with high flux. *Adv. Mater.* **25**, 2071 (2013)
  29. D. Li, X. Gou, D. Wu, Z. Guo, A robust and stretchable superhydrophobic PDMS/PVDF@KNFs membrane for oil/water separation and flame retardancy. *Nanoscale* **10**, 6695 (2018)
  30. P. Jin, C. Huang, Y. Li, J. Li, L. Wang, Fabrication of a superhydrophobic poly(vinylidene fluoride) hollow fibre membrane by spray deposition. *Micro. Nano Lett.* **13**, 223 (2018)
  31. C. Wei, F. Dai, L. Lin, Z. An, Y. He, X. Chen, L. Chen, Y. Zhao, Simplified and robust adhesive-free superhydrophobic SiO<sub>2</sub>-decorated PVDF membranes for efficient oil/water separation. *J. Membr. Sci.* **555**, 220 (2018)
  32. H. Sun, Y. Xu, Y. Zhou, W. Gao, H. Zhao, W. Wang, Preparation of superhydrophobic nanocomposite fiber membranes by electrospinning poly(vinylidene fluoride)/silane coupling agent modified SiO<sub>2</sub> nanoparticles. *J. Appl. Polym. Sci.* **44501**, 1 (2017)
  33. M. Toh, P. Oh, T. Chew, A. Ahmad, Antiwettability enhancement of PVDF-HFP membrane via superhydrophobic modification by SiO<sub>2</sub> nanoparticles. *C. Chim.* **22**, 369 (2019)
  34. L.-N. Nthunya, L. Gutierrez, A.-R. Verliefd, S.-D. Mhlanga, Enhanced flux in direct contact membrane distillation using superhydrophobic PVDF nanofibre membranes embedded with organically modified SiO<sub>2</sub> nanoparticles. *J Chem Technol Biotechnol.* **94**, 2826 (2019)
  35. S. Wang, Y. Li, X. Fei, M. Sun, C. Zhang, Y. Li, Q. Yang, X. Hong, Preparation of a durable superhydrophobic membrane by electrospinning poly(vinylidene fluoride)(PVDF) mixed with epoxy-siloxane modified SiO<sub>2</sub> nanoparticles: a possible route to superhydrophobic surfaces with low water sliding angle and high water contact angle. *J. Colloid Interface Sci.* **359**, 380 (2011)
  36. M. Mohammadi, M. Tembely, A. Dolatabadi, Predictive model of supercooled water droplet pinning/repulsion impacting a superhydrophobic surface: the role of the gas-liquid interface temperature. *Langmuir* **33**, 1816 (2017)
  37. Z. Wang, A. Yang, X. Tan, Y. Tu, S. Sabin, P. Xiang, M. Wang, R. Guo, X. Chen, A veil-over-sprout micro-nano PMMA/SiO<sub>2</sub> superhydrophobic coating with impressive abrasion, icing, and corrosion resistance. *Colloids Surf. A.* **601**, 124998 (2020)
  38. V. Bahadur, L. Mishchenko, B. Hatton, J. Taylor, J. Aizenberg, T. Krupenkin, Predictive Model for Ice Formation on Superhydrophobic Surfaces. *Langmuir* **27**, 14143 (2011)
  39. N. Fletcher, J. Hasted, The Chemical Physics of Ice. *Phys. Today.* **24**, 49 (1971)
  40. X. Wu, W. Wang, Theoretical analysis of initial behavior of frost formed on a cold surface. *J Eng Thermophys.* **24**, 286 (2003)
  41. R. Dou, J. Chen, Y. Zhang, X. Wang, D. Cui, Y. Song, L. Jiang, J. Wang, Anti-icing coating with an aqueous lubricating layer. *ACS Appl. Mater. Interfaces.* **6**, 6998 (2014)
  42. C. Lv, H. Wang, Z. Liu, W. Zhang, C. Wang, R. Tao, M. Li, Y. Zhu, A sturdy self-cleaning and anti-corrosion superhydrophobic coating assembled by amino silicon oil modifying potassium titanate whisker-silica particles. *Appl. Surf. Sci.* **435**, 903 (2018)
  43. X. Chen, J. Yuan, J. Huang, K. Ren, Y. Liu, S. Lu, H. Li, Large-scale fabrication of superhydrophobic polyurethane/nano-Al<sub>2</sub>O<sub>3</sub> coatings by suspension flame spraying for anti-corrosion applications. *Appl. Surf. Sci.* **311**, 864 (2014)